# Effect of irradiation on microstructure and hardening of Cr–Fe–Ni–Mn high-entropy alloy and its strengthened version

V.N. Voyevodin, S.A. Karpov, G.D. Tolstolutskaya, M.A. Tikhonovsky, A.N. Velikodnyi, I.E. Kopanets, G.N. Tolmachova, A.S. Kalchenko, R.L. Vasilenko & I.V. Kolodiy

Published online: 19 Dec 2019.

Submit your article to this journal ⃗

View related articles ⃗

View Crossmark data ⃗

Taylor & Francis
Taylor & Francis Group

Check for updates

# Effect of irradiation on microstructure and hardening of Cr–Fe–Ni–Mn high-entropy alloy and its strengthened version

V.N. Voyevodin[a,b], S.A. Karpov[a], G.D. Tolstolutskaya[a], M.A. Tikhonovsky[a], A.N. Velikodnyi[a], I.E. Kopanets[a], G.N. Tolmachova[a], A.S. Kalchenko[a], R.L. Vasilenko[a] and I.V. Kolodiy [a]

[a]National Science Centre 'Kharkov Institute of Physics and Technology', Kharkov, Ukraine; [b]V.N. Karazin Kharkiv National University, Kharkov, Ukraine

**ABSTRACT**

A single-phase fcc high-entropy alloy (HEA) of 20%Cr–40%Fe–20%Mn–20%Ni composition and its strength with yttrium and zirconium oxides version was irradiated with 1.4 MeV Ar ions at room temperature and mid-range doses from 0.1 to 10 displacements per atom (dpa). Transmission electron microscopy (TEM), scanning transmission electron microscopy with energy dispersive X-ray spectrometry (STEM/EDS) and X-ray diffraction (XRD) were used to characterise the radiation defects and microstructural changes. Nanoindentation was used to measure the ion irradiation effect on hardening. In order to understand the irradiation effects in HEAs and to demonstrate their potential advantages, a comparison was performed with hardening behaviour of 316 austenitic stainless steel irradiated under an identical condition. It was shown that hardness increases with irradiation dose for all the materials studied, but this increase is lower in high-entropy alloys than in stainless steel.

## 1. Introduction

Establishing of fusion and GEN IV fission reactors defines new materials challenges in terms of higher operating temperatures, higher neutron exposures, as well as ensuring safe and efficient operation. High-entropy alloys are a new effort in materials science and engineering. These alloys have multiple metallic elements of nearly equimolar compositions and stabilised solid solution phases. The higher configurational entropy leads to reduce the tendency of forming intermetallic phases at high temperatures. It was shown that HEAs have excellent strength and resistance to corrosion, wear, and softening at high temperatures because the diffusion kinetics in HEAs is suggested to be sluggish [1,2].

---

**CONTACT** S.A. Karpov ✉ karpofff@kipt.kharkov.ua 💬 National Science Centre 'Kharkov Institute of Physics and Technology', Kharkov, Ukraine

It is supposed that these features of structure and diffusion kinetics might influence point defect recombination phenomena in irradiated materials, which can increase structural and radiation stability, and provide self-healing ability under irradiation conditions compared to conventional single-phase alloys [3–5].

Radiation stability, mechanical and tribological properties can be enhanced by the use of metal matrix composite HEA with $Y_2O_3$ as the reinforcement phase. Nanosized oxide (NO) particles that are dispersed in the matrix act as pinning points for dislocation motion and grain boundaries movement, which consequently have significant effects on the microstructure stability and mechanical properties [6]. Moreover, in almost all cases, an increase in strength characteristics leads to a significant decrease in ductility. It is necessary to find a balance, which in turn requires a profound understanding of the effect of radiation damage on hardening achieved by fundamental research on and examination of a significant number of materials. However, knowledge of their irradiation response is very limited, since the research and development of these alloys just started.

Part of the high-entropy alloys studied to date contains Co, making them unfavourable for nuclear applications due to high neutron transmutation-induced radioactivity. It can increase radiation shielding requirements during handling after neutron exposure.

In the present study, a non-cobalt 20Cr–40Fe–20Mn–20Ni (mass. %) high-entropy alloy and its strengthened with yttrium and zirconium oxides version have been investigated. The key objective of this study is to investigate these alloys in relation to the hardening/embrittlement phenomenon under irradiation. The dependence of the hardening parameters on the irradiation dose, their relationship with the evolution of the microstructure is studied. Comparison of the obtained data with that for conventional stainless steel 316 is done.

## 2. Materials and methods

High-entropy alloy with the nominal composition of 20Cr–40Fe–20Mn–20Ni were produced by arc melting in a water-cooled copper mould filled with high-purity argon. The purity of the alloying elements was above 99.9%. To ensure chemical homogeneity, the ingots were flipped over and re-melted a least five times. The produced ingots had dimensions of about 6×15×60 mm. Homogenisation annealing of these ingots was performed at 850°C for 24 h. Prior to homogenisation samples were sealed in vacuumed ($10^{-2}$ Torr) quartz tubes filled with titanium chips to prevent oxidation. Alloys were subjected to thermomechanical treatment (TMT) that consisted of deformation by rolling at room temperature from 6 to 0.5 mm. Finishing annealing of 0.5 mm specimens was carried out at 850°C for 1 h.

The process of mechanical alloying of HEA powders with oxides and receiving 20Cr–40Fe–20Mn–20Ni–ODS powders was carried out in a ball mill in an inert atmosphere of argon [7]. 15 g of alloy powder with a dispersion of ≤300 μm was placed into a steel container of a high-energy planetary ball mill and 0.5% (mass) a pre-synthesised powder of composition 80% $Y_2O_3$ + 20% $ZrO_2$ (in mol%) with a dispersion of about 14 nm was added. The rotation speed and time of mechanical alloying were 460 rpm and 4 h, respectively. The synthesised powder was compacted by cold pressing, followed by sintering in vacuum at a temperature of 1100°C for 30 min. Then, the billets were rolled into a 0.5 mm thick strip with intermediate annealing at 850°C. At the final stage, the strip was annealed at 1100°C for 1 h.

Solution annealed commercial type 316 stainless steel with typical composition has been used in the current study as a reference austenitic material.

Surfaces of the samples were mechanically polished initially with sandpapers of varying grits and finally electrolytically polished using 95% methanol and 5% perchloric acid solution at a temperature of −20°C with an applied voltage of 30 V to remove mechanically damaged layer.

Samples of all three materials with dimensions of $10 \times 5 \times 0.5$ mm were irradiated with 1.4 MeV argon ions at room temperature (RT) in a dose range of 0.1–10 dpa. These mid-range doses are evaluated at a depth of ∼0.25 μm. All irradiations were carried out with the accelerating-measuring system 'ESU-2' [8], which contain Van de Graaf accelerator. The depth distribution of Ar atoms concentration and damage was calculated by SRIM 2008 [9] and shown in Figure 1. The damage calculations are based on the Kinchin–Pease model (KP), with a displacement energy for each alloying element was set to 40 eV, as recommended in ASTM E521-96 (2009) [10].
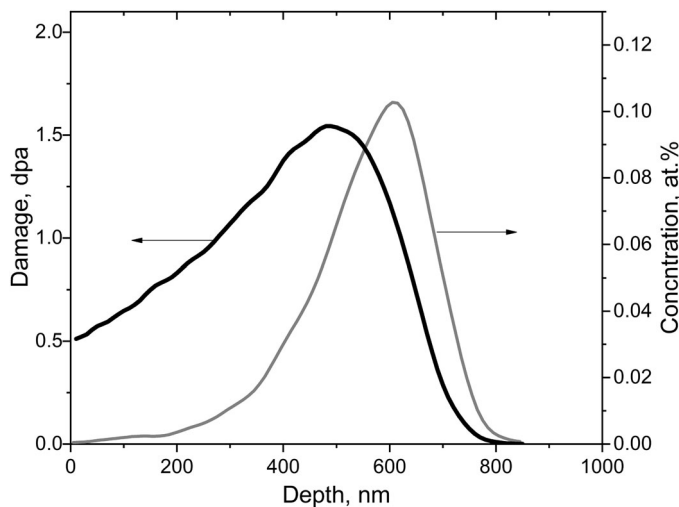


**Figure 1.** Calculated profiles of damages and concentrations of 1.4 MeV Ar ions in alloy 20Cr–40Fe–20Mn–20Ni irradiated to a dose of $2.2 \times 10^{15}$ cm$^{-2}$.

Nanohardness was measured by Nanoindenter G200 with a Berkovich type indentation tip. A 'continuous stiffness measurement method' was used [11], which produces mechanical property data as a function of indenter depth. Tests were performed with a constant deformation rate of $0.05\ s^{-1}$. Each sample was applied at least 10 prints at a distance of 35 μm from each other. The methodology of Oliver & Pharr was used to find the hardness [12].

The crystal structure of the alloys was studied by X-ray diffractometry (Dron-4, Cu $K_\alpha$ radiation). Transmission electron microscopy (TEM, JEOL, JEM-2100) equipped with energy dispersive X-ray spectrometry (EDS) was used to characterise the radiation defects and microstructural changes. Secondary electron images produced in scanning electron microscopy (SEM, JEOL, JSM-6710F) were used for investigations of as-received and irradiated specimens in regions surrounding indents.

The procedure of electron microscopy specimen preparation involved electrochemically polishing the ion-incident surface to ensure no mechanical damage was present. Following irradiation, a pulse electropolishing procedure was used to remove $50 \pm 5$ nm from the ion-incident surface. While protecting this surface, the back surface was electropolished until perforation occurred at the front surface to yield electron-transparent areas for transmission microscopy.

Convergent beam electron diffraction (CBED) has been applied for HEAs thickness measurements. Processing of obtained CBED patterns was performed with the software package provided by Klinger [13].

## 3. Results and discussion

### 3.1. Pre-irradiation characterisation

Figure 2 shows the typical microstructure of a non-cobalt 20Cr–40Fe–20Mn–20Ni high-entropy alloy and its strengthened version. According to X-ray analysis, both as-cast alloys and alloys after TMT and final heat treatment at 1100°C are single-phase with fcc crystal lattice. The average grain size of HEA and ODS-HEA were almost an order of magnitude smaller than SS316 and were estimated to be 3.47 and 1.61 μm, respectively. The initial dislocation density in all studied alloys was varied from $1.7 \times 10^{12}$–$2.5 \times 10^{12}\ m^{-2}$. The chemical compositions for each alloy are specified in Table 1.

Figure 3 shows the bright-field STEM image of precipitates and EDS mapping of ODS–20Cr–40Fe–20Mn–20Ni high-entropy alloy. It is clearly visible that there are two kinds of precipitates in the matrix according to the chemical composition. The larger ones marked by arrows are the Cr–Mn–O rich precipitates. Smaller precipitates contain elements of Y and Zr. The compositional analysis performed by means of energy dispersive spectroscopy (EDS) has indicated that these precipitates are $(Y,Zr)_2O_3$ [Figure 4(a)].
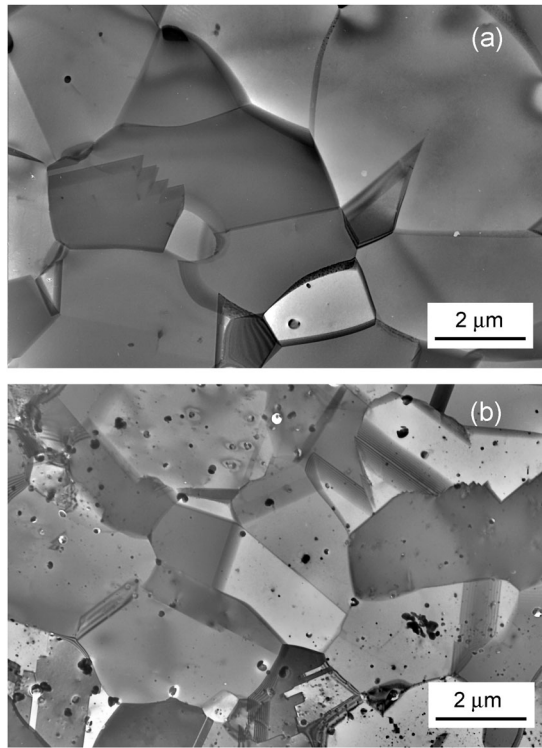
**Figure 2.** Typical TEM micrograph of (a) 20Cr–40Fe–20Mn–20Ni, (b) ODS–20Cr–40Fe–20Mn–20Ni high-entropy alloys.

**Table 1.** Nominal and measured material compositions (wt. %).

|              | Fe    | Cr     | Ni     | Mn    | Mo    | Si    | Y     | Zr    | O     |
| ------------ | ----- | ------ | ------ | ----- | ----- | ----- | ----- | ----- | ----- |
| **FeCrNiMn** |       |        |        |       |       |       |       |       |       |
| Nominal      | 40    | 20     | 20     | 20    | –     | –     | –     | –     | –     |
| Measured     | 41.1  | 18     | 21.8   | 19.1  | –     | –     | –     | –     | –     |
| **ODS–FeCrNiMn** |   |        |        |       |       |       |       |       |       |
| Nominal      | 39.5  | 20     | 20     | 20    | –     | –     | 0.4   | 0.1   | –     |
| Measured     | 43.4  | 18.6   | 18.4   | 17.7  | –     | –     | 0.48  | 0.22  | 1.2   |
| **SS316**    |       |        |        |       |       |       |       |       |       |
| Nominal      | Bal.  | 16–18  | 10–14  | 2.0   | 2–3   | 1.0   | –     | –     | –     |
| Measured     | Bal.  | 17.3   | 12.53  | 1.77  | 2.4   | 0.68  | –     | –     | –     |

The different areas of TEM foil were examined in order to investigate the distribution of the nanosized oxides [Figure 4(b)]. The minimum and maximum oxides diameter were 2.0 and 90 nm; the highest fraction of NO was estimated at about 50% for NO with diameters close to 20.0 nm, and overall NO number density was $3.0 \times 10^{21}$ m$^{-3}$.

## 3.2. Irradiation effects on microstructure

TEM micrographs in Figure 5 show the microstructural evolution of HEAs and SS316 irradiated with 1.4 MeV argon ions at room temperature to 1 dpa. All
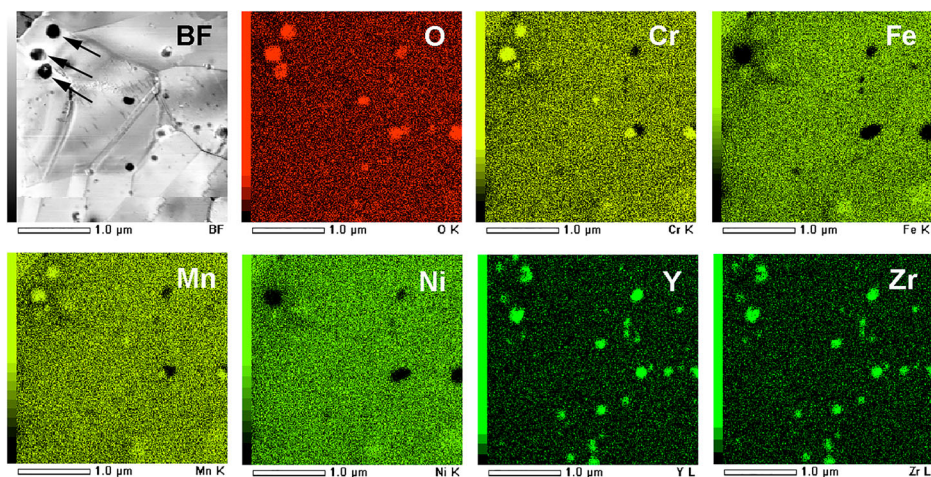
**Figure 3.** BF STEM image and EDS mapping of ODS–20Cr–40Fe–20Mn–20Ni high-entropy alloy.

images were recorded under bright-field down-zone imaging conditions at [011] axis zone. Irradiated samples showed significant changes in the microstructure as compared to the unirradiated sample. The main irradiation defects observed were defect clusters at low doses and dislocation loops at higher doses. The defect clusters became visible at relatively low doses (<0.1 dpa KP). Tilting experiments clearly showed the dislocation nature of observed defects.

According to [14], radiation-induced dislocation loops in HEAs are typically interstitial loops. It was previously shown that loops produced in SS316 under irradiation with 1.4 MeV Ar ions at RT are faulted Frank loops with Burgers vectors of $b = a_0/3\langle 111 \rangle$ lying on {111} planes [15]. The HEAs in this study share similar crystal structure and constituent elements with SS316 and may have the same loop characteristics.

The evolution of dislocation loops vs. doses found to be similar in the HEA and SS316, while somewhat different in ODS-HEA. The average size of defects in the latter case is noticeably smaller. The densities of 'black spots' at 1 dpa are estimated to be $7 \times 10^{22}$, $6 \times 10^{22}$ and $1.2 \times 10^{23}$ m$^{-3}$ for HEA, ODS-HEA alloys and SS316, respectively.

## 3.3. Irradiation hardening

Figure 6 shows nanoindentation hardness of ODS-HEA alloy as a function of indenter displacement before and after ion irradiation with argon ions to 5 dpa. The irradiation with Ar ions at RT leads to an increase of nanohardness. In all samples, the first 100 nm of displacement shows a considerable increase in the scatter of the data due to tip-rounding artefacts and surface preparation effects. Therefore, for all samples, the first 100 nm of data will be ignored for the remainder of the analysis.
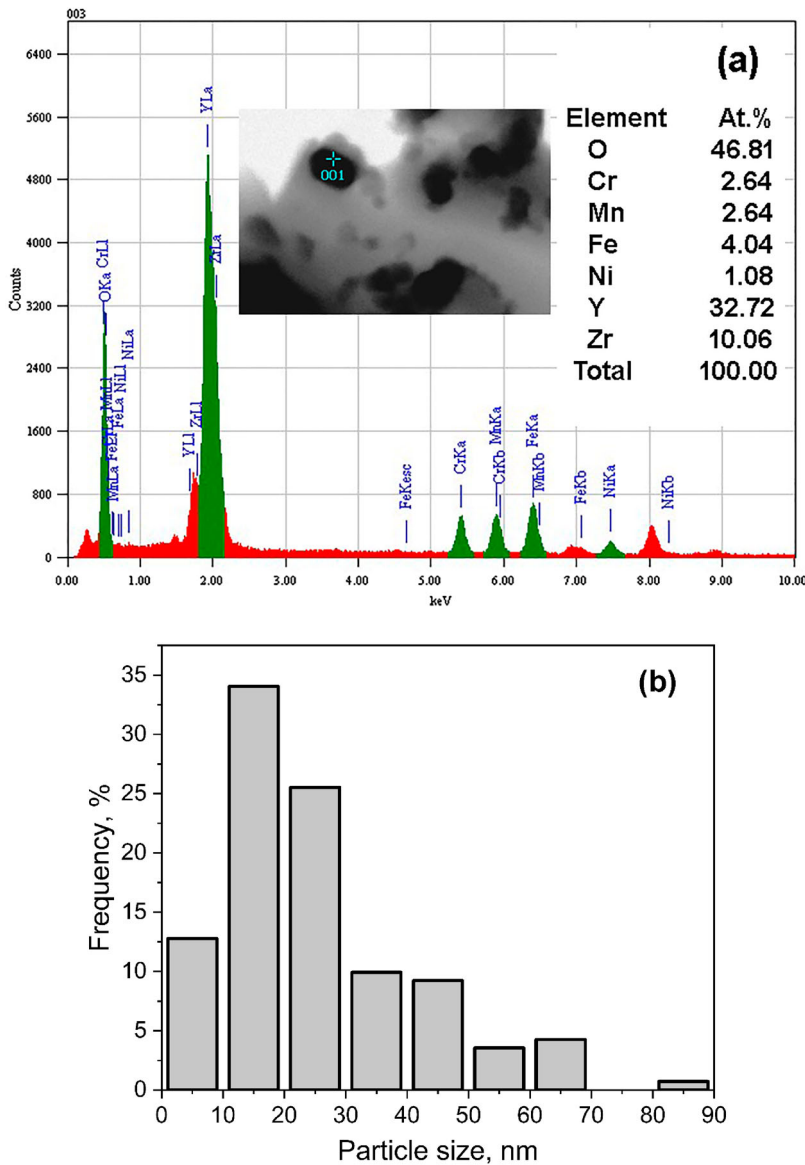
**Figure 4.** (a) EDX spectra and results of quantitative analysis of the inclusions in ODS-HEA alloy, (b) size distribution of $(Y,Zr)_2O_3$ oxides.

Generally, the indentation hardness of ion-irradiated materials represents the superposition of the bulk hardness, indentation size effect (ISE) and the irradiation-induced hardening [16]. The analysis method by nanoindentation measurement is based on the Nix–Gao model [17] that describes the concept of geometrically necessary dislocations required to accommodate the indenter together with Kasada method [18] that extended model [17] by a film-substrate system based on so-called the soft substrate effect. The ion-irradiated materials, according to [18], can be considered as 'hardened layer–substrate' systems. The
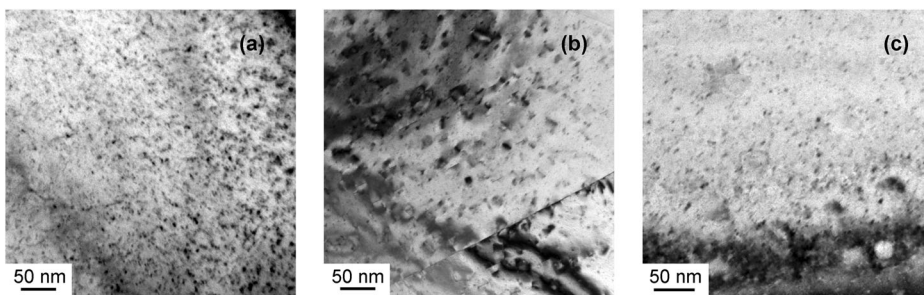
**Figure 5.** TEM micrographs of (a) 20Cr–40Fe–20Mn–20Ni, (b) ODS–20Cr–40Fe–20Mn–20Ni high-entropy alloys and (c) SS316 irradiated at room temperature with 1.4 MeV Ar ions to 1 dpa.
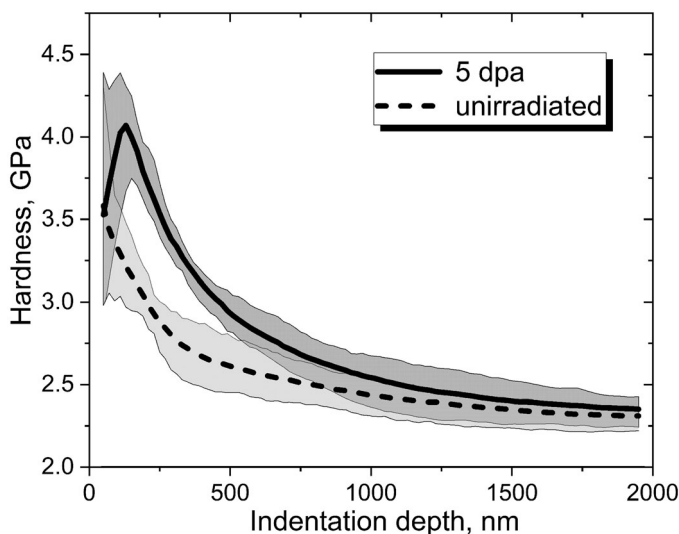


**Figure 6.** Indentation hardness as a function of contact depth for unirradiated and 1.4 MeV $Ar^+$-irradiated ODS–20Cr–40Fe–20Mn–20Ni high-entropy alloy.

unirradiated region below the irradiated layer will be plastically deformed before the indenter itself reaches the unirradiated region. The transition point of one area to another represents the critical indentation depth $h_c$, and the bulk-equivalent hardness, $H_0^{irr}$, of the ion-irradiated region can be obtained by the least square fitting of the hardness data up to a critical depth $h_c$.

By redrawing the hardness profile in terms of Nix–Gao plot (squared hardness vs. reciprocal depth), the bulk-equivalent hardness of the ion-irradiated region has been evaluated (Figure 7). In the case of unirradiated alloy, Nix–Gao plot represents virtually a straight line due to the lack of a radiation-hardened layer.

The nanohardness of the unirradiated samples, $H_0^{as-received}$, was calculated to be $1.71 \pm 0.11$, $2.11 \pm 0.15$, $2.21 \pm 0.15$ GPa for HEA, ODS-HEA, and SS316, respectively. The increase in nanohardness of ODS-HEA caused by grain size
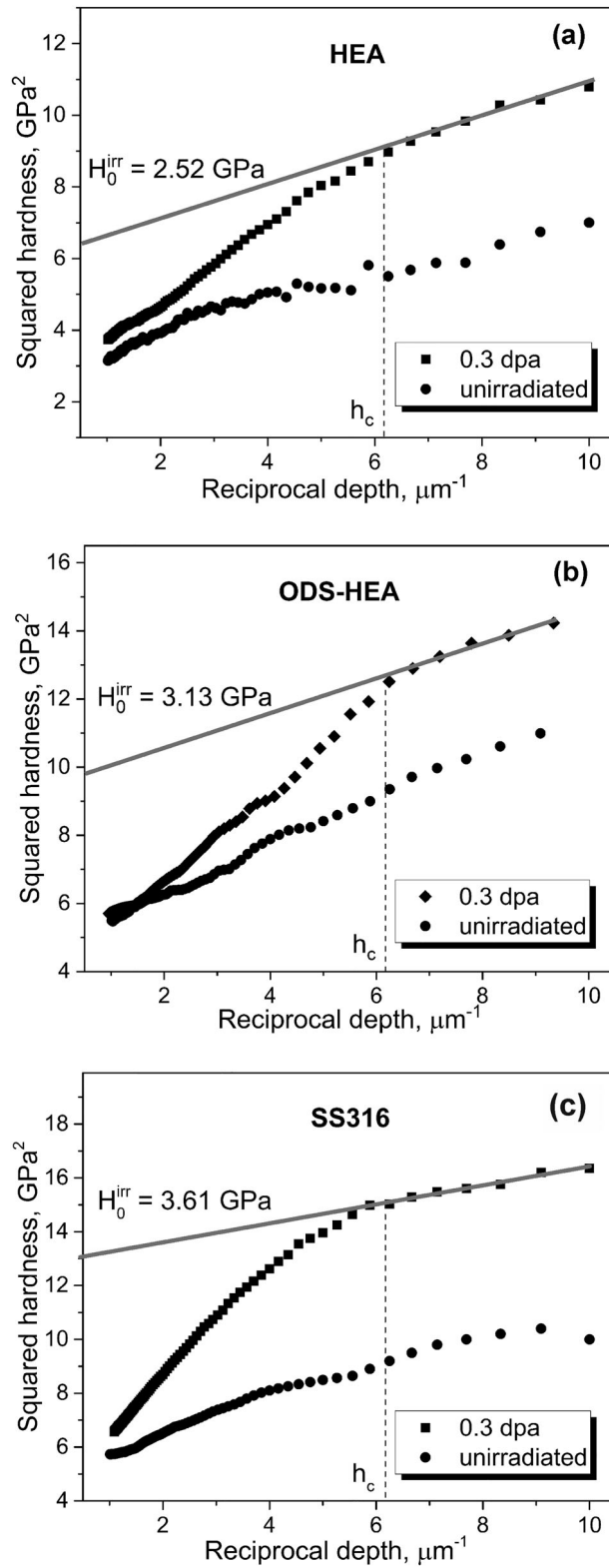
**Figure 7.** Nix–Gao plot for unirradiated and argon irradiated for 0.3 dpa (a) HEA, (b) ODS-HEA, and SS316.

reduction and addition of yttrium and zirconium oxides is more than 20% in comparison with the base HEA.

It should be noted, that at determining the bulk-equivalent hardness for both as-received and irradiated material using the method of Oliver and Pharr the additional effects of pile-up/sink-in of testing material around the indent must be taken into account. After indentation, the hardness impressions were imaged using SEM to control contact areas. According to Figure 8, the imprint of the indenter correlates well with the triangular area defined by the edges of indenter [see Figure 8(b,d)]. So, the effect of pile-up was not observed and the effect of sink-in of testing material around the indent was insignificant and not taken into account at processing data on nanoindentation.

Figure 9 represents the dose dependences of bulk-equivalent hardness (points) for as-received and irradiated HEAs, and SS316 as a reference material. The uncertainty of the measured hardness equals one standard deviation of the hardness data. The nanohardness of all examined materials increases with damaging dose over the entire range of doses studied: most pronounced in the low-dose range with a gradual quasi-saturation at higher fluencies.

Approximations of hardness values by a power function of the form $H_0^{irr} = H_0^{as-received} + m(dpa)^n$, where $m$ and $n$ are fitting coefficients, are also shown (solid lines) in Figure 9. According to previous studies [19,20], the parameter n is typically close to 0.1 at a high dose. By setting n equal to 0.1 for all cases, the hardness dependencies fit perfectly when m is equal to 1.0, 1.1, and 1.7 for HEA, ODS-HEA, and SS316, respectively.

The nanohardness increments, $\Delta H$, defined by the difference between the irradiated and unirradiated samples, $\Delta H = H_0^{irr} - H_0^{as-received}$, is graphed in Figure 10. Irradiated HEA has minimum nanohardness increments, while $\Delta H$ of ODS-HEA is 15–25% higher than the HEA. Taking into account that the yield stress of materials is proportional to the hardness and hardening $\Delta \sigma_y = K\Delta H$ [21], it can be deduced that hardening increases with irradiation dose, and the largest hardening is detected in SS316.

Irradiated samples showed significant changes in the microstructure relatively the unirradiated sample – the very small-sized 'black spots' and dislocation loops were observed (see Figure 5). Recent studies [22] have shown that the clusters of
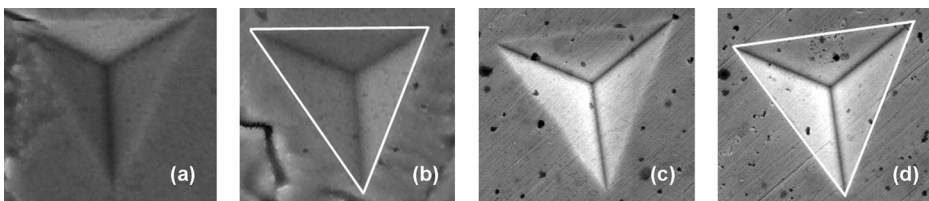


**Figure 8.** SEM images showing regions surrounding indents in unirradiated (a,c) and irradiated (b,d) regions. (a,b) HEA, (c,d) ODS-HEA.
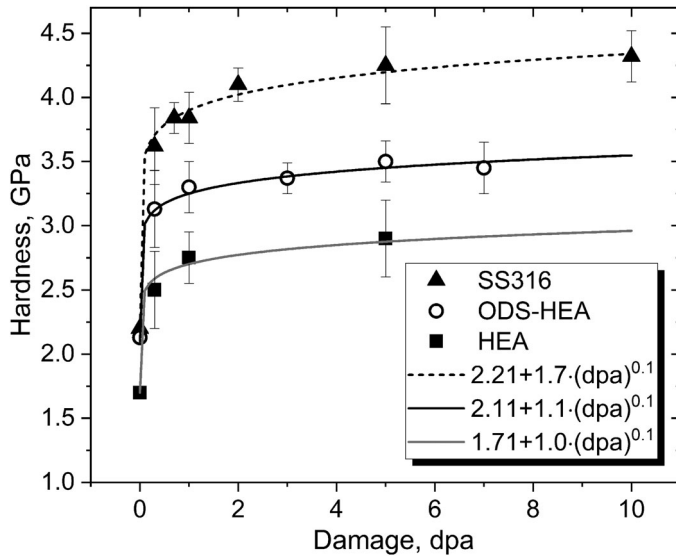
**Figure 9.** The dose dependence of bulk-equivalent hardness of ion-irradiated HEA, ODS-HEA alloys and SS316.
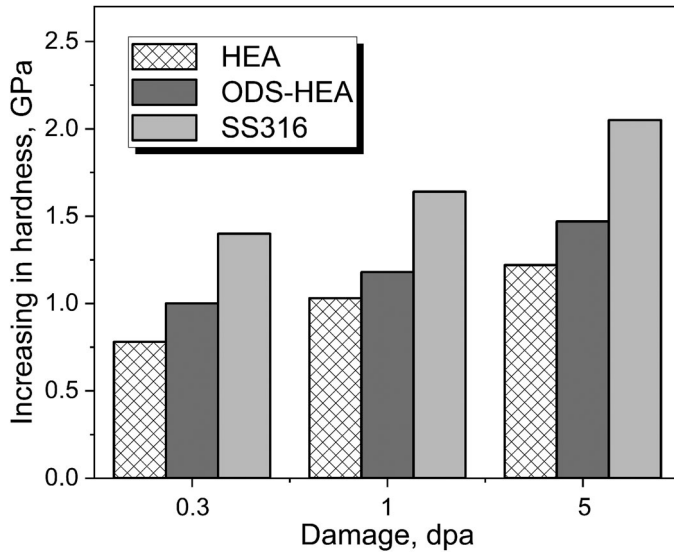


**Figure 10.** Nanohardness increments of the irradiated HEA, ODS-HEA alloys and SS316.

defects and dislocation loops appeared in HEA materials as early as 0.01 dpa, and the density increased with increasing dose until about 0.1–1 dpa when the density gradually saturated. This is consistent with the results of work [23] after low-temperature irradiation experiments on FeNiMnCr high-entropy alloy.

The formation and evolution of irradiation-induced defect clusters and dislocation loops are an important factor for irradiation hardening. The effect of dislocation loops on hardening in the case of HEAs requires verification, but it is expected that a higher configurational entropy, highly distorted lattice, and more sluggish diffusion kinetics can result in a smaller mean size and lower density of dislocation loops, and consequently to a decrease in radiation hardening [22]. Unfortunately, few results about the evolution of irradiation-induced dislocation loops with doses are inconsistent among recent studies. In [24] a general tendency of decreasing loop density and increasing loop size with the enhancement of compositional complexity under 1 MeV krypton ion irradiations to 2 dpa at 773 K was reported. Although previously [25], an opposite trend for the same materials irradiated at similar temperatures with $Ni^{2+}$ ions has been observed.

Comparing HEAs with austenitic steels, authors [23] have demonstrated that the dislocation loops were smaller while density higher in irradiated HEAs than in SS316. Chen et al. performed the irradiation of two high-entropy alloys, $Al_{0.3}$-CoCrFeNi and CoCrMnFeNi, and a 316H SS with 1 MeV krypton ions to 1 dpa at 300°C with *in situ* TEM observations [22]. An analysis of radiation-induced microstructure exhibited that the size and density evolutions of dislocation loops were similar for the HEAs and 316H. The increase in nanoindentation hardness after irradiation was about 1 GPa for both HEAs and 316H. The authors made the assumption that such similar behaviours of HEAs and 316H under irradiation are due to most dislocation loops were formed as a result of cascade collapsing where the long-range diffusion of point defects is negligible.

The results of this study showed that the densities of 'black spots' at 0.3–5 dpa are somewhat lower in HEA than in SS316. Despite the conclusions [22], the present result suggests that at least factors of high configurational entropy and highly distorted lattice played a certain role in the microstructural evolution of HEAs at low irradiation temperatures.

Nanosized oxide particles dispersed in the matrix, as the reinforcement phase, can enhance microstructure stability and mechanical properties of HEA alloy. According to [26], the strengthening mechanism of ODS-HEA can be attributed to: (i) grain boundary strengthening, which can be explained by Hall–Petch relationship; (ii) dispersion strengthening; and (iii) load transfer effect. In this paper, alloying component in the composition of 80% $Y_2O_3$ + 20% $ZrO_2$ ensured the excess of ~20% in hardening of initial ODS-HEA as compared with HEA under the impact of a combination of specified factors.

An increase in radiation-induced hardening of ODS-HEA is 15–25% higher than the HEA in the entire range of doses studied, despite the fact that the density of visible dislocation loops is lower in ODS-HEA. It can be assumed that in this case, in addition to the pinning effect of dislocation loops, oxides

also have an effect [27,28]. Future work on the irradiation effects on ODS-HEA should focus on establishing the causes of this phenomenon. Nevertheless, results obtained in this work indicate that the processes of hardening/embrittlement will develop in HEAs and ODS-HEAs much slower than conventional Fe–Cr–Ni austenitic alloys.

## 4. Conclusions

In the present experimental study, a non-cobalt 20Cr–40Fe–20Mn–20Ni (wt. %) high-entropy alloy and its strengthened with yttrium and zirconium oxides version have been investigated in relation to the development of hardening phenomenon under the irradiation. The irradiation effects in HEAs were compared with hardening behaviour of 316 austenitic stainless steel irradiated under an identical condition. The main conclusions are as follows:

1. Initial high-entropy alloy reinforced with the mixture of yttrium and zirconium oxides in the composition of 80% $Y_2O_3$ and 20% $ZrO_2$ provided an excess of about 20% in nanohardness as compared with base HEA.
2. The nanohardness of all studied materials increases with damaging dose and approaches the quasi-saturation mode at high fluencies. The dose dependencies of hardness for HEAs and SS316 fit well by the simple power function with the same exponent of 0.1.
3. Irradiated HEA and ODS-HEA demonstrate a lower increase in radiation-induced nanohardness as compared with SS316. These observations suggest that high-entropy alloys must lose less plasticity in comparison with conventional austenitic steels of nuclear power.

## Disclosure statement

## ORCID

*I.V. Kolodiy* 🟢 http://orcid.org/0000-0001-8598-9732

## References

[1] J.W. Yeh, Y.L. Chen and S.J. Lin, *High-entropy alloys – a new era of exploitation*. Mater. Sci. Forum 560 (2007), pp. 1–9.
[2] D.B. Miracle and O.N. Senkov, *A critical review of high entropy alloys and related concepts*. Acta Mater. 122 (2017), pp. 448–511.
[3] M. Tsai and J. Yeh, *High-entropy alloys: a critical review*. Mater. Res. Lett. 2 (2014), pp. 107–123.

[4] Y. Zhang, G. Stocks and K. Jin, *Influence of chemical disorder on energy dissipation and defect evolution in concentrated solid solution alloys*. Nat. Commun. 6 (2015), p. 8736.

[5] C. Lu, L. Niu and N. Chen, *Enhancing radiation tolerance by controlling defect mobility and migration pathways in multicomponent single-phase alloys*. Nat. Commun. 7 (2016), pp. 13564.

[6] C. Lu, Z. Lu and X. Wang, *Enhanced radiation-tolerant oxide dispersion strengthened steel and its microstructure evolution under helium-implantation and heavy-ion irradiation*. Sci. Rep. 7 (2017), pp. 1–7.

[7] S.V. Starostenko, V.M. Voyevodin and M.A. Tykhonovs'kyi, *Microstructure of 08Kh18N10 T austenitic steel mechanically alloyed with nanooxides of the $Y_2O_3$-$ZrO_2$ system*. Mater. Sci. 51 (2016), pp. 822–832.

[8] G.D. Tolstolutskaya, V.V. Ruzhytskiy and I.E. Kopanetz, *Accelerating complex for study of helium and hydrogen behavior in conditions of radiation defects generation*. Probl. Atom. Sci. Tech. 1 (2010), pp. 135–140.

[9] SRIM (2008), http://www.srim.org/

[10] ASTM E521-96 (2009), ASTM.

[11] G.N. Tolmachova, G.D. Tolstolutskaya and S.A. Karpov, *Application of nanoindentation for investigation of radiation damage in SS316 stainless steel*. Probl. Atom. Sci. Tech. 5 (2015), pp. 168–173.

[12] W.C. Oliver and G.M. Pharr, *An improved technique for determining hardness and elastic modulus using load and displacement sensing indentation experiments*. J. Mater. Res. 7 (1992), pp. 1564–1583.

[13] M. Klinger, *More features, more tools, more CrysTBox*. J. Appl. Cryst. 50 (2017), pp. 1226–1234.

[14] M.-R. He, S. Wang and K. Jin, *Enhanced damage resistance and novel defect structure of CrFeCoNi under in situ electron irradiation*. Scripta Mater. 125 (2016), pp. 5–9.

[15] B.S. Sungurov, G.D. Tolstolutskaya and S.A. Karpov, *Characterization of dislocation type defects formed at low-energy deuterium irradiation of SS316 stainless steel*. Probl. Atom. Sci. Tech. 2 (2018), pp. 8–12.

[16] M. Saleh, Z. Zaidi and M. Ionescu, *Relationship between damage and hardness profiles in ion irradiated SS316 using nanoindentation – experiments and modeling*. Int. J. Plast. 86 (2016), pp. 151–169.

[17] W.D. Nix and H.J. Gao, *Indentation size effects in crystalline materials: A law for strain gradient plasticity*. J. Mech. Phys. Solids 46 (1998), pp. 411–425.

[18] R. Kasada, Y. Takayama and K. Yabuuchi, *A new approach to evaluate irradiation hardening of ion-irradiated ferritic alloys by nano-indentation techniques*. Fusion Eng. Des. 86 (2011), pp. 2658–2661.

[19] S.A. Karpov, G.D. Tolstolutskaya and B.S. Sungurov, *Hardening of SS316 stainless steel caused by the irradiation with argon ions*. Mater. Sci. 52 (2016), pp. 377–384.

[20] T.S. Byun and K. Farrell, *Irradiation hardening behaviour of polycrystalline metals after low temperature irradiation*. J. Nucl. Mater. 326 (2004), pp. 86–96.

[21] J.T. Busby, M.C. Hash and G.S. Was, *The relationship between hardness and yield stress in irradiated austenitic and ferritic steels*. J. Nucl. Mater. 336 (2005), pp. 267–278.

[22] W.-Y. Chen, X. Liu and Y. Chen, *Irradiation effects in high entropy alloys and 316H stainless steel at 300°C*. J. Nucl. Mater. 510 (2018), pp. 421–430.

[23] N.K. Kumar, C. Li and K. Leonard, *Microstructural stability and mechanical behavior of FeNiMnCr high entropy alloy under ion irradiation*. Acta Mater. 113 (2016), pp. 230–244.

[24] S. Shi, M.-R. He and K. Jin, *Evolution of ion damage at 773 K in Ni- containing concentrated solid-solution alloys*. J. Nucl. Mater. 510 (2018), pp. 132–142.

[25] C. Lu, T. Yang and K. Jin, *Radiation-induced segregation on defect clusters in single-phase concentrated solid-solution alloys.* Acta Mater. 127 (2017), pp. 98–107.

[26] R. Casati and M. Vedani, *Metal matrix composites reinforced by nano-particles – a review.* Metals 4 (2014), pp. 65–83.

[27] H. Kim, J. Gigax and T. Chen, *Dispersoid stability in ion irradiated oxide-dispersion-strengthened alloy.* J. Nucl. Mater. 509 (2018), pp. 504–512.

[28] J.P. Wharry, M.J. Swenson and K.H. Yano, *A review of the irradiation evolution of dispersed oxide nanoparticles in the b.c.c. Fe-Cr system: current understanding and future directions.* J. Nucl. Mater. 486 (2017), pp. 11–20.